C–H•••F–C Interactions: A Guide for Designing Fluorous Monodentate Ligands for the Highly Linear-Selective Hydroformylation at Near-Ambient Pressure

Yuchao Deng
CAS Key Lab of Low-Carbon Conversion Science and Engineering, Shanghai Advanced Research Institute, Chinese Academy of Sciences https://orcid.org/0000-0003-0843-7517

Xiaofang Liu
CAS Key Lab of Low-Carbon Conversion Science and Engineering, Shanghai Advanced Research Institute, Chinese Academy of Sciences

Baiyin Wei
CAS Key Lab of Low-Carbon Conversion Science and Engineering, Shanghai Advanced Research Institute, Chinese Academy of Sciences

Zhimin Zhou
CAS Key Lab of Low-Carbon Conversion Science and Engineering, Shanghai Advanced Research Institute, Chinese Academy of Sciences

Kaimin Hua
CAS Key Lab of Low-Carbon Conversion Science and Engineering, Shanghai Advanced Research Institute, Chinese Academy of Sciences

Junjun Chen
CAS Key Lab of Low-Carbon Conversion Science and Engineering, Shanghai Advanced Research Institute, Chinese Academy of Sciences

Shenggang Li
CAS Key Lab of Low-Carbon Conversion Science and Engineering, Shanghai Advanced Research Institute, Chinese Academy of Sciences

Hui Wang (wanghh@sari.ac.cn)
CAS Key Lab of Low-Carbon Conversion Science and Engineering, Shanghai Advanced Research Institute, Chinese Academy of Sciences https://orcid.org/0000-0002-6536-5188

Xiao Wang (wanghh@sari.ac.cn)
School of Chemistry and Chemical Engineering, Nanjing University https://orcid.org/0000-0002-7748-5670

Yuhan Sun (sunyh@sari.ac.cn)
CAS Key Lab of Low-Carbon Conversion Science and Engineering, Shanghai Advanced Research Institute, Chinese Academy of Sciences https://orcid.org/0000-0002-2940-213X

Research Article

Keywords: fluorinated molecules, C–H•••F–C interactions, hydroformylation

Posted Date: May 24th, 2021

DOI: https://doi.org/10.21203/rs.3.rs-550969/v1

Abstract

Organofluorine compounds often exhibit unique catalytic capabilities with novel structural scaffold, reactivity and mechanisms. Herein, we report a Rh-catalyzed hydroformylation under mild conditions using monodentate phosphite ligands $P(OCH_2CF_3)_3$ (TTFP) and $P(OCH_2CF_2CH_3)_3$ (TDFP). The ligand were designed with the principle that the inclusion of fluorine-rich group can significantly change the physical and chemical properties of the complex through H•••F hydrogen bonds, the existence of which has been confirmed by crystal-packing studies. These monodentate phosphite ligands self-assemble to form bidentate ligands through C–H•••F–C interactions, and catalysts based on these ligands deliver extremely high regioselectivities in hydroformylation. Aldehydes were formed with up to 92% chemoselectivity, with linear aldehydes formed in high regioselectivity (*n:iso*=28/1) under a syngas pressure of only 2 atm.

Background

Fluorinated molecules have unique and important physicochemical properties[1,2], which have been used extensively to develop medicines[3,4] and agrochemicals[5,6]. The introduction of fluorine alters the physicochemical properties of a molecule by changing its chemical reactivity and the stability of adjacent functional groups, as well as its pK_a and dipole moment[4,7,8]. Fluorous interactions (C–F···F–C, C–H···F–C, C–H···π) have been reported to significantly influence the arrangements of molecules in molecular crystals [9-11], photophysical[12] and solvation properties[13]. Several reported studies aimed at understanding the nature of these interactions, including approaches based on statistical analysis[14], energy calculations[14], crystal structure analysis[15] and charge-density analysis[16]. The different statistical-analysis-based surface area correction approaches[17] have been applied to C–H···F–C and C–F···F–C interactions, revealing that the lighter fluorine halogen favors the C–H···F–C interactions[18,19]. The nature of C–H···F–C interactions in molecular crystals has been exhaustively investigated, and it behaves as a weak hydrogen bond that is dominated by electrostatic and dispersion components when the two fragments are neutral [15,20]. The C–H···F–C hydrogen bond plays an important role in the formation of self-assembled adlayers during crystal packing[10], with intermolecular, molecule-substrate, and intramolecular interactions the driving forces that dominate the self-assembled structure. With this in mind, we asked the question: can these in-situ-generated interactions be applied to homogeneous catalytic reactions?

Hydroformylation is one of the most important homogeneous chemical processes, which converts olefins into aldehydes. Novel catalysts with improved efficiency have been continually developed over the past four decades. Rh-based catalysts modified by phosphorus ligands are widely used, and the development of ligands has become the optimal way to improve the catalytic activity. In contrast to their monodentate counterparts, bidentate donor ligands generally lead to higher regio- and enantioselectivities in many homogeneous transition-metal catalysts due to the formation of a more rigid microenvironment at the catalytic metal center[21,22]. Ligands that self-assemble[23] via O–H···O and N–H···N hydrogen bonds

to form a psuedo bidentate ligand has been reported to facilitate hydroformylation in a regioselective manner. Fluorous interactions can also be used to increase rigidity in the microenvironment of the catalytic metal center, thereby increasing the selectivity of the reaction. Generating a monodentate ligand with hydrogen bond donor/acceptor is more cost-effective than preparing a bidentate ligand with tedious synthetic steps[24].

Monosubstituted $HRh(CO)_3L$ catalysts used in ethylene hydroformylation have been computationally simulated by the Jensen group[25] using density functional theory (DFT), which elucidated the electronic and steric factors governing the catalytic activity of the modified phosphite ligand (L). Electron-withdrawing ligands, such as $P(OCH_2CF_3)_3$, were predicted to be more active than those used for contemporary hydroformylation. Taken together the results of previous experimental[26,27] and computational studies[25,28] on Rh-catalyzed hydroformylation, we designed a set of fluorine-containing monodentate phosphite ligands in the present work. Experimental and computational studies suggest that these ligands self-assemble through the C–H···F–C interaction that increases the rigidity of the microenvironment around the Rh center and more effectively distinguishes between the reaction pathways for selectively forming linear aldehydes.

Results And Discussion

Initial Experiments and Optimizations

Fluorine-containing ligands were confirmed to exhibit high regioselectivity for linear aldehydes compared to other monodentate ligands through an initial set of experiments that used 1-decene as a benchmark substrate and various monodentate ligands in toluene under 2 atm of syngas at 70 °C (Figure 1). As triphenylphosphine (TPP) is widely used in industry, we first examined ligands **L2** and **L3**, which are TPP derivatives with electron-withdrawing CF_3 groups. However, no satisfactory results were obtained (entries 2 and 3). Under the abovementioned mild conditions, partially fluorinated ligands **L4**–**L6** provided the same level of regioselectivity as Biphephos (**L1**), a classical and prominent bidentate ligand for hydroformylation (entries 1 and 4–7); however, the highest linear-to-branched aldehyde ratio (*n:iso*=40.1:1) was observed with **L7** (entry 7).

With the optimal fluorine-containing ligands **L4**–**L7**, we set to explore hydroformylation conditions using these ligands (Supplementary Information, Table S1–S4). We observed that the proportion of fluorine-containing ligand is a decisive factor for the linear selectivity (Figure 2). The *n:iso* ratios above 10/1 were observed at L/Rh ratios above 5:1, which is higher than the regioselectivity observed for most currently used monodentate ligands. The desired undecaldehyde was obtained in excellent isolated yields, with 91% yield and 96% regioselectivity observed using 2.5 mol% tris(2,2-difluoropropyl)phosphite (TDFP, L/[Rh]=5).

Reaction conditions: $Rh(acac)(CO)_2$ (0.5 mol%), $P(CO/H_2=1:1)$ = 2 atm, 1-decene (2 mmol), toluene (1 mL), T = 70 ℃, t = 16 h. Selectivity of aldehydes and *n:iso* ratios were determined by GC-MS with an

internal standard (*n*-dodecane). *n*-aldehyde% = linear aldehyde selectivity.

Substrate Scope and Comparison with PPh_3 and TPPTS Ligands

With the optimal ligand in hand, we compared TTFP and TDFP with the widely used PPh_3 and the water-soluble monodentate ligand TPPTS. High yields and linear selectivities were obtained for C6–C10 olefins when the electron-withdrawing TTFP and TDFP ligands were used (Figure 3). Under the same conditions, the water-soluble TPPTS provided high regioselectivities (>84%), however the yields were below 50% (Figure 3). While the industrially relevant PPh_3 delivered an aldehyde yield of more than 85%, only 70–83% undecanal was obtained under mild hydroformylation conditions. By carefully optimizing the reaction conditions, we found that TDFP exhibited good catalytic activities and linear aldehyde selectivities for aliphatic olefin. However, TDFP did not work satisfactorily for aromatic olefins or internal olefins (Table S5–S7). The highly regioselective hydroformylations of terminal olefins suggest that specific interactions exist between these fluorine-containing monodentate ligands, and that these interactions remain intact during the catalytic process.

Reaction conditions: [a] **L**[TTFP or TDFP]/[Rh]=5:1, **L**(TPPTS or PPh_3)/[Rh]=3:1, 1-decene (2 mmol), toluene (1 mL), P(CO/H_2=1:1) = 2 atm, *T* = 70°C, t = 16 h. GC yield and *n:iso* ratios were calculated by GC-MS with an internal standard (*n*-dodecane). *n%* = linear aldehyde selectivity. [b] Isolated yield. [c] Solvent: V (CH_3CH_2OH): V (H_2O) = 2/3–1 (1 mL).

Mechanistic Investigation

Wilkinson's widely accepted dissociation mechanism (Figure 4a)[29,30] is followed by most Rh-catalyzed hydroformylation reactions, in which regioselectivity is determined by olefin insertion at a trigonal-bipyramidal five-coordinate intermediate. According to the experimental results and calculated free energies of the stationary points in the hydroformylation catalyzed by $HRh(CO)_3$(TTFP) reported by Jensen et al.[25], olefin insertion into the metal–H bond requires high energy (**2** → **3** or **3'**). The bite angle of the phosphite ligand and the rigidity of the microenvironment at the Rh center of transition state **2** are key factors that affect aldehyde regioselectivity during hydroformylation[31,32]. It should be noted here that some of the reported computational work supports the notion that electron-withdrawing ligands are associated with low activation energies and trigonal-bipyramidal transition-state geometries[25,33,34]. The complete structures of Rh/TTFP complexes with phosphorus ligands containing hydrolysable bonds (e.g., P–O) and non-rigid groups are difficult to obtain by X-ray diffractometry. Therefore, alkene intermediate **2**, which contains two bis-equatorially coordinated phosphorus ligands, was examined computationally.

Computational studies of intermediate **2"** with 1-butene as the substrate were carried out using the Gaussian 09 suite of programs[35]. The geometries of all molecules were optimized using the B3LYP[36-38] and BP86[39,40] density functional with the Stuttgart-Dresden effective core potential (ECP28MWB) with the associated double-ζ basis set[41] for Rh and the 6-31G**[42] basis set used for all other elements. The

solvation effect of toluene was incorporated through the self-consistent reaction field (SCRF) approach using the integral equation formalism of the polarizable continuum model (IEFPCM). The nature of each optimized structure was determined by frequency calculations.

The computational studies revealed the existence of intramolecular C–H···F–C hydrogen bonding interactions in the Rh catalyst modified with the fluorinated ligands. The optimized structures of [RhH(CO)(1-butene)$\mathbf{L}_2$] and those of weak hydrogen bonding combinations are depicted in Figure 4b-d, with selected optimized bond distances and angles of alkene intermediate **2"** listed in Table S8. We screened H···F distances below 2.7 Å (the sum of the van der Waals radii of H and F)[43] that correspond to intramolecular C–H···F–C interactions between the two ligands. It should be noted here that H···F distances for C–H···F–C interactions reported in the literature range between 2.00 and 4.00 Å[17]. The H···F distances between the two ligands were determined to lie in the 2.20–2.70 Å range (Table S8) with C–H···F and H···F–C angles of 90–180° (Table S9). The H···F interactions correspond to weak hydrogen bonds in these distance and angle ranges[17]. The optimized structures of alkene intermediates **2"** bearing the TTFP and TDFP ligands (Figures 4b and 4c) reveal that the C–H bonds involved in H···F interactions are shorter than other C–H bonds on the same carbon atom, which is consistent with C–H bond shortening due to short-range repulsion. Moreover, a short distance in the 2.4–2.6 Å range was observed between the fluorine and the α-hydrogen of 1-butene. The formation of C–H···F–C hydrogen bonds increases the rigidity of the microenvironment at the Rh center, with a P–Rh–P angle within the 100–110° range to energetically discriminate between competing reaction pathways, thus leads to higher regioselectivity[21,44]. This was consistent with our experimental results.

Furthermore, the FTIR peaks that correspond to the C–F and C–H bonds in the fluorine-containing monodentate TTFP and TDFP were blue-shifted when Rh(acac)$(CO)_2$ was added ($n_L/n_{[Rh]}$=1, 3, 5 and 7). The FTIR spectra at the optimized [Rh]/L ratio (1:5) (Figure 5, spectra in red) exhibited a blue-shift of 3 cm^{-1}. Taken together with the DFT-optimized structure, we speculate that these shifts are due to the formation of C–H···F–C hydrogen bonds. A large number of studies into the blue-shifting C–H···X–type (X=F, Cl, N, O)[45-47] hydrogen bonding have been reported over the past two decades, and the magnitude of the blue-shift is the key factor that distinguishes it from conventional hydrogen bonding.

Conclusions

In conclusion, we have designed a class of monodentate fluorine-containing phosphite ligands that are able to self-assemble through C–H···F–C interactions to form “pseudo” bidentate ligands. The Rh catalyst modified with the TTFP or TDFP ligand was proved highly active and regioselective for hydroformylation under extremely mild conditions. Experimental data and computational studies reveal that C–H···F–C hydrogen bonds are the key to the extremely high regioselectivity. Further synthetic applications of the C–H···F–C interactions are currently being investigated in our laboratory.

Methods

General procedure for the hydroformylation at near-ambient pressure

Procedure A

In a 5 mL vial equipped with a magnetic bar was added Rh(acac)$(CO)_2$ (0.01 mmol), ligand (0.01-0.1 mmol), alkene (2 mmol) and toluene (1 mL). After stirring for 5 min, the vial was transferred into an autoclave and replaced air with syngas over 5 times. Syngas (CO/H_2=1:1, 1-2 atm) were charged in autoclave. The reaction mixture was stirred at 60-100 °C (oil bath) for 16 h. The pressure was carefully released in a fume hood after the reaction was cooled. The internal standard (*n*-dodecane, 1 mmol) was added to the collected reaction mixture (2 mmol scale). GC yield and *n:iso* ratios were calculated by GC-MS with an internal standard (*n*-dodecane).

Procedure B

In a 5 mL vial equipped with a magnetic bar was added Rh(acac)$(CO)_2$ (0.01 mmol), ligand TDFP (0.05 mmol), alkene (2 mmol) and toluene (1 mL). After stirring for 5 min, the vial was transferred into an autoclave and replaced air with syngas over 5 times. Syngas (CO/H_2=1:1, 2 atm) were charged in autoclave. The reaction mixture was stirred at 70 °C (oil bath) for 16 h. The pressure was carefully released in a fume hood after the reaction was cooled. The collected reaction mixture (2 mmol scale) was dried under reduced pressure, and the mixture was subjected to column chromatography (silica gel, *n*-pentane/ether) to afford pure product. The final product was weighed and characterized by ^{1}H NMR and GC-MS.

Data and code availability

There is no dataset and code associated with the paper. Characterization and spectra are included in the Supplemental information.

Declarations

Acknowledgements

We acknowledge financial support from the National Natural Science Foundation of China (21776296, 21905291 and 21872068), the National Key Research and Development Program of China (2017YFB0602203), the Strategic Priority Research Program of the Chinese Academy of Sciences (XDA21090201), and the Shanghai Sailing Program (19YF1453000).

Author contributions

Y.D., H.W., X.W. and Y.S. designed and developed this project. Y.D. performed the catalytic experiments and data analysis. Y.D., X.L., X.W. and H.W. wrote the manuscript. Y.D., Z.Z. and S.L. performed computational studies. B.W., K.H. and J.C. performed some experiments and discussed the work.

Competing interests

The authors declare no competing interests.

References

1 Clot, E. *et al.* C–F and C–H bond activation of fluorobenzenes and fluoropyridines at transition metal centers: How fluorine tips the scales. *Acc. Chem. Res.***44**, 333-348 (2011).

2 Amii, H. & Uneyama, K. C–F bond activation in organic synthesis. *Chem. Rev.***109**, 2119-2183 (2009).

3 Müller, K., Faeh, C. & Diederich, F. Fluorine in pharmaceuticals: looking beyond intuition. *Science***317**, 1881-1886 (2007).

4 Purser, S., Moore, P. R., Swallow, S. & Gouverneur, V. Fluorine in medicinal chemistry. *Chem. Soc. Rev.***37**, 320-330 (2008).

5 Fujiwara, T. & O'Hagan, D. Successful fluorine-containing herbicide agrochemicals. *J. Fluorine Chem.***167**, 16-29 (2014).

6 Theodoridis, G. in *Advances in Fluorine Science* Vol. 2 (ed Alain Tressaud) 121-175 (Elsevier, 2006).

7 Zhou, Y. *et al.* Next generation of fluorine-containing pharmaceuticals, compounds currently in phase II–III clinical trials of major pharmaceutical companies: New structural trends and therapeutic Areas. *Chem. Rev.***116**, 422-518 (2016).

8 Salwiczek, M., Nyakatura, E. K., Gerling, U. I. M., Ye, S. & Koksch, B. Fluorinated amino acids: Compatibility with native protein structures and effects on protein–protein interactions. *Chem. Soc. Rev.***41**, 2135-2171 (2012).

9 Reichenbächer, K., Süss, H. I. & Hulliger, J. Fluorine in crystal engineering—"the little atom that could". *Chem. Soc. Rev.***34**, 22-30 (2005).

10 Rohde, D., Yan, C.-J. & Wan, L.-J. C–H···F hydrogen bonding: The origin of the self-assemblies of bis(2,2'-difluoro-1,3,2-dioxaborine). *Langmuir***22**, 4750-4757 (2006).

11 Han, Z. *et al.* Imaging the halogen bond in self-assembled halogenbenzenes on silver. *Science***358**, 206-210 (2017).

12 Zhang, G., Lu, J., Sabat, M. & Fraser, C. L. Polymorphism and reversible mechanochromic luminescence for solid-state difluoroboron avobenzone. *J. Am. Chem. Soc.***132**, 2160-2162 (2010).

13 Takamuku, T., Yamamoto, M., To, T. & Matsugami, M. Solvation structures of tetraethylammonium bromide and tetrafluoroborate in aqueous binary solvents with ethanol, trifluoroethanol, and acetonitrile. *J. Phys. Chem. B***124**, 5009-5020 (2020).

14 Gavezzotti, A. & Presti, L. L. Building blocks of crystal engineering: A large-database study of the intermolecular approach between C–H donor groups and O, N, Cl, or F acceptors in organic crystals. *Cryst. Growth Des.***16**, 2952-2962 (2016).

15 Marten, J., Seichter, W., Weber, E. & Böhme, U. Crystalline packings of diketoarylhydrazones controlled by a methyl for trifluoromethyl structural change. *CrystEngComm***10**, 541-547 (2008).

16 Choudhury, A. R. & Guru Row, T. N. How realistic are interactions involving organic fluorine in crystal engineering? Insights from packing features in substituted isoquinolines. *Cryst. Growth Des.***4**, 47-52 (2004).

17 Saha, B. K., Saha, A., Sharada, D. & Rather, S. A. F or O, Which one is the better hydrogen bond (Is it?) acceptor in C–H···X–C (X– = F–, O) interactions? *Cryst. Growth Des.***18**, 1-6 (2018).

18 van den Berg, J.-A. & Seddon, K. R. Critical evaluation of C–H···X hydrogen bonding in the crystalline state. *Cryst. Growth Des.***3**, 643-661 (2003).

19 Ibrahim, M. A. A. & Moussa, N. A. M. Unconventional type III halogen···halogen interactions: A quantum mechanical elucidation of σ-hole···σ-hole and Di-σ-hole interactions. *ACS Omega***5**, 21824-21835 (2020).

20 Loader, J. R., Libri, S., Meijer, A. J. H. M., Perutz, R. N. & Brammer, L. Highly fluorinated naphthalenes and bifurcated C–H···F–C hydrogen bonding. *CrystEngComm***16**, 9711-9720 (2014).

21 Bronger, R. P., Kamer, P. C. & van Leeuwen, P. W. Influence of the bite angle on the hydroformylation of internal olefins to linear aldehydes. *Organometallics***22**, 5358-5369 (2003).

22 van der Veen, L. A. *et al.* Electronic effect on rhodium diphosphine catalyzed hydroformylation: The bite angle effect reconsidered. *J. Am. Chem. Soc.***120**, 11616-11626 (1998).

23 Breit, B. & Seiche, W. Hydrogen bonding as a construction element for bidentate donor ligands in homogeneous catalysis: regioselective hydroformylation of terminal alkenes. *J. Am. Chem. Soc.***125**, 6608-6609 (2003).

24 Ustynyuk, Y. A., Babin, Y. V., Savchenko, V. G., Myshakin, E. M. & Gavrikov, A. V. Mechanism of ethylene hydroformylation on platinum complexes with hydrophosphoryl ligands: a DFT study. *Russ. Chem. Bull.***59**, 686-694 (2010).

25 Sparta, M., Børve, K. J. & Jensen, V. R. Activity of Rhodium-Catalyzed Hydroformylation: Added Insight and Predictions from Theory. *J. Am. Chem. Soc.***129**, 8487-8499 (2007).

26 Horváth, I. T. *et al.* Molecular engineering in homogeneous catalysis: One-phase catalysis coupled with biphase catalyst separation. The fluorous-soluble $HRh(CO)\{P[CH_2CH_2(CF_2)_5CF_3]_3\}_3$ hydroformylation system. *J. Am. Chem. Soc.***120**, 3133-3143 (1998).

27 Wilhelmus, P., Van Leeuwen, N. M. & Roobeek, C. F. A process for the hydroformylation of olefins. United Kingdom patent GB2068377 (1981).

28 Dingwall, P. *et al.* Understanding a hydroformylation catalyst that produces branched aldehydes from alkyl alkenes. *J. Am. Chem. Soc.***139**, 15921-15932 (2017).

29 Brown, C. K. & Wilkinson, G. Homogeneous hydroformylation of alkenes with hydridocarbonyltris-(triphenylphosphine)rhodium(I) as catalyst. *J. Chem. Soc. A*, 2753-2764 (1970).

30 Evans, D., Osborn, J. A. & Wilkinson, G. Hydroformylation of alkenes by use of rhodium complex catalysts. *J. Chem. Soc. A*, 3133-3142 (1968).

31 Luo, X. *et al.* Mechanism of rhodium-catalyzed formyl activation: A computational study. *J. Org. Chem.***81**, 2320-2326 (2016).

32 Shaharun, M. S., Dutta, B. K. & Mukhtar, H. Ab initio energy calculations and macroscopic rate modeling of hydroformylation of higher alkenes by Rh-based catalyst. *AIChE J.***55**, 3221-3233 (2009).

33 Fristrup, P., Kreis, M., Palmelund, A., Norrby, P.-O. & Madsen, R. The mechanism for the rhodium-catalyzed decarbonylation of aldehydes: A combined experimental and theoretical study. *J. Am. Chem. Soc.***130**, 5206-5215 (2008).

34 Zuidema, E., Daura-Oller, E., Carbó, J. J., Bo, C. & van Leeuwen, P. W. N. M. Electronic ligand effects on the regioselectivity of the rhodium−diphosphine-catalyzed hydroformylation of propene. *Organometallics***26**, 2234-2242 (2007).

35 Frisch, M. J. *et al.* **Gaussian, Inc., Wallingford CT** (2016).

36 Becke, A. D. Density-functional thermochemistry. III. The role of exact exchange. *J. Chem. Phys.***98**, 5648-5652 (1993).

37 Lee, C., Yang, W. & Parr, R. G. Development of the Colle-Salvetti correlation-energy formula into a functional of the electron density. *Phys. Rev. B***37**, 785-789 (1988).

38 Vosko, S. H., Wilk, L. & Nusair, M. Accurate spin-dependent electron liquid correlation energies for local spin density calculations: a critical analysis. *Can. J. Phys.***58**, 1200-1211 (1980).

39 Becke, A. D. Density-functional exchange-energy approximation with correct asymptotic behavior. *Phys. Rev. A***38**, 3098-3100 (1988).

40 Perdew, J. P. Density-functional approximation for the correlation energy of the inhomogeneous electron gas. *Phys. Rev. B***33**, 8822-8824 (1986).

41 Peterson, K. A., Figgen, D., Dolg, M. & Stoll, H. Energy-consistent relativistic pseudopotentials and correlation consistent basis sets for the 4d elements Y–Pd. *J. Chem. Phys.***126**, 124101 (2007).

42 Pritchard, B. P., Altarawy, D., Didier, B., Gibson, T. D. & Windus, T. L. New basis set exchange: An open, up-to-date resource for the molecular sciences community. *J. Chem. Inf. Model.***59**, 4814-4820 (2019).

43 Bondi, A. van der Waals Volumes and Radii. *J. Phys. Chem.***68**, 441-451 (1964).

44 Kamer, P. C., Van Leeuwen, P. W. & Reek, J. N. Wide bite angle diphosphines: Xantphos ligands in transition metal complexes and catalysis. *Acc. Chem. Res.***34**, 895-904 (2001).

45 Karpfen, A. & Kryachko, E. S. Blue-shifted hydrogen-bonded complexes. II. $CH_3F\cdots(HF)_{1\leqslant n\leqslant 3}$ and $CH_2F_2\cdots(HF)_{1\leqslant n\leqslant 3}$. *Chem. Phys.***310**, 77-84 (2005).

46 Matsuura, H. *et al.* Experimental evidence for intramolecular blue-shifting C–H···O hydrogen bonding by matrix-isolation infrared spectroscopy. *J. Am. Chem. Soc.***125**, 13910-13911 (2003).

47 Rodziewicz, P., Rutkowski, K. S., Melikova, S. M. & Koll, A. Cooperative effects in blue-shifted hydrogen bonded cluster of $CF_3H\cdots(HF)_{1\leqslant n\leqslant 3}$ from first principles simulations. *Chem. Phys.***361**, 129-136 (2009).

Figures

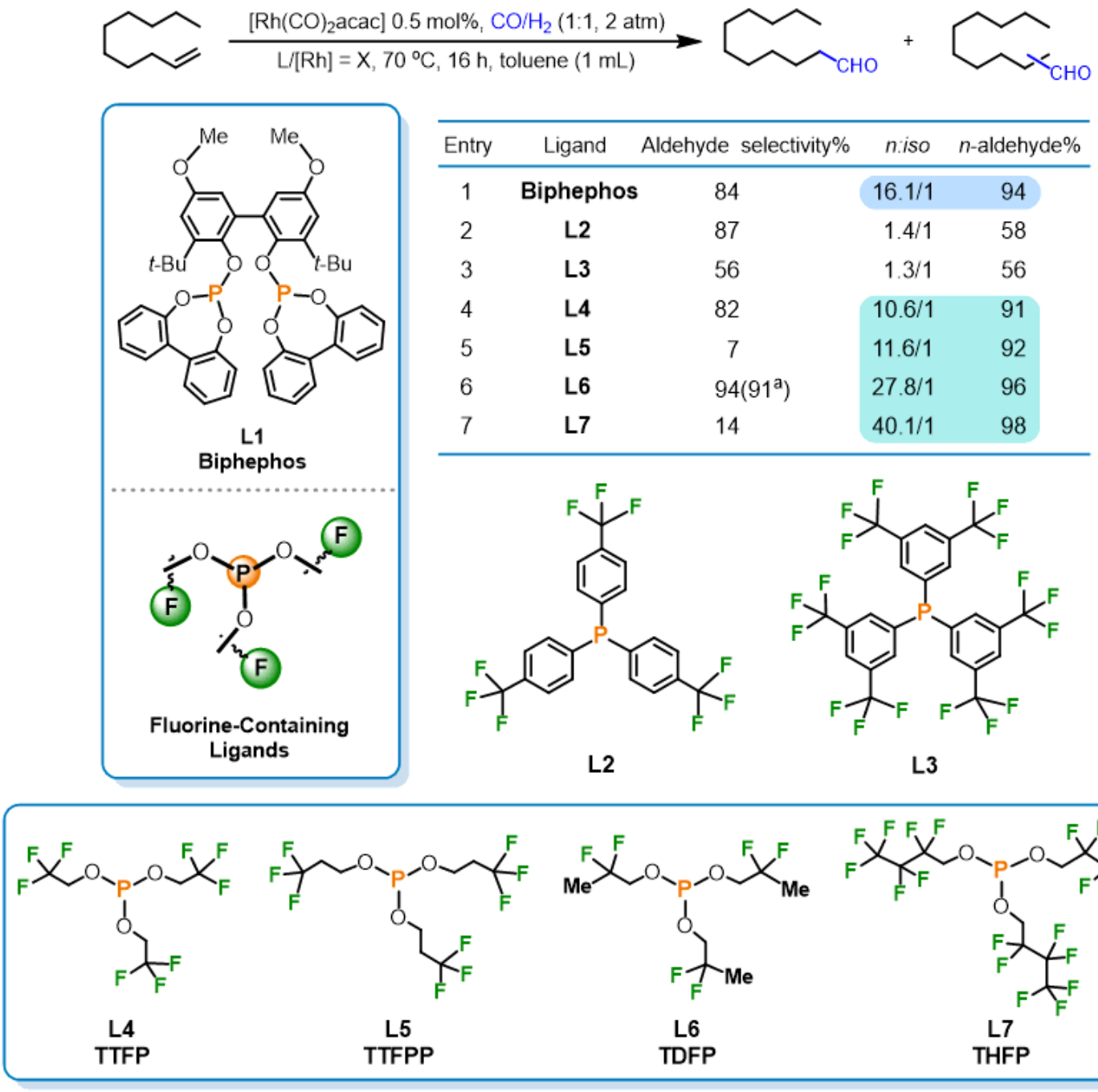

Entry	Ligand	Aldehyde selectivity%	*n:iso*	*n*-aldehyde%
1	**Biphephos**	84	16.1/1	94
2	**L2**	87	1.4/1	58
3	**L3**	56	1.3/1	56
4	**L4**	82	10.6/1	91
5	**L5**	7	11.6/1	92
6	**L6**	94(91[a])	27.8/1	96
7	**L7**	14	40.1/1	98

Figure 1

Optimizing the monodentate ligand for the hydroformylation of 1-decene. Reaction conditions: Rh(acac)(CO)2 (0.5 mol%), L1/[Rh]=3:1, L(2-7)/[Rh]=5:1, 1-decene (2 mmol), toluene (1 mL), P(CO/H2=1:1) = 2 atm, T = 70 °C, t = 16 h. Selectivity of aldehydes and n:iso ratios were determined by GC-MS with an internal standard (n-dodecane). n- aldehyde% = linear aldehyde selectivity. a Isolated yield.

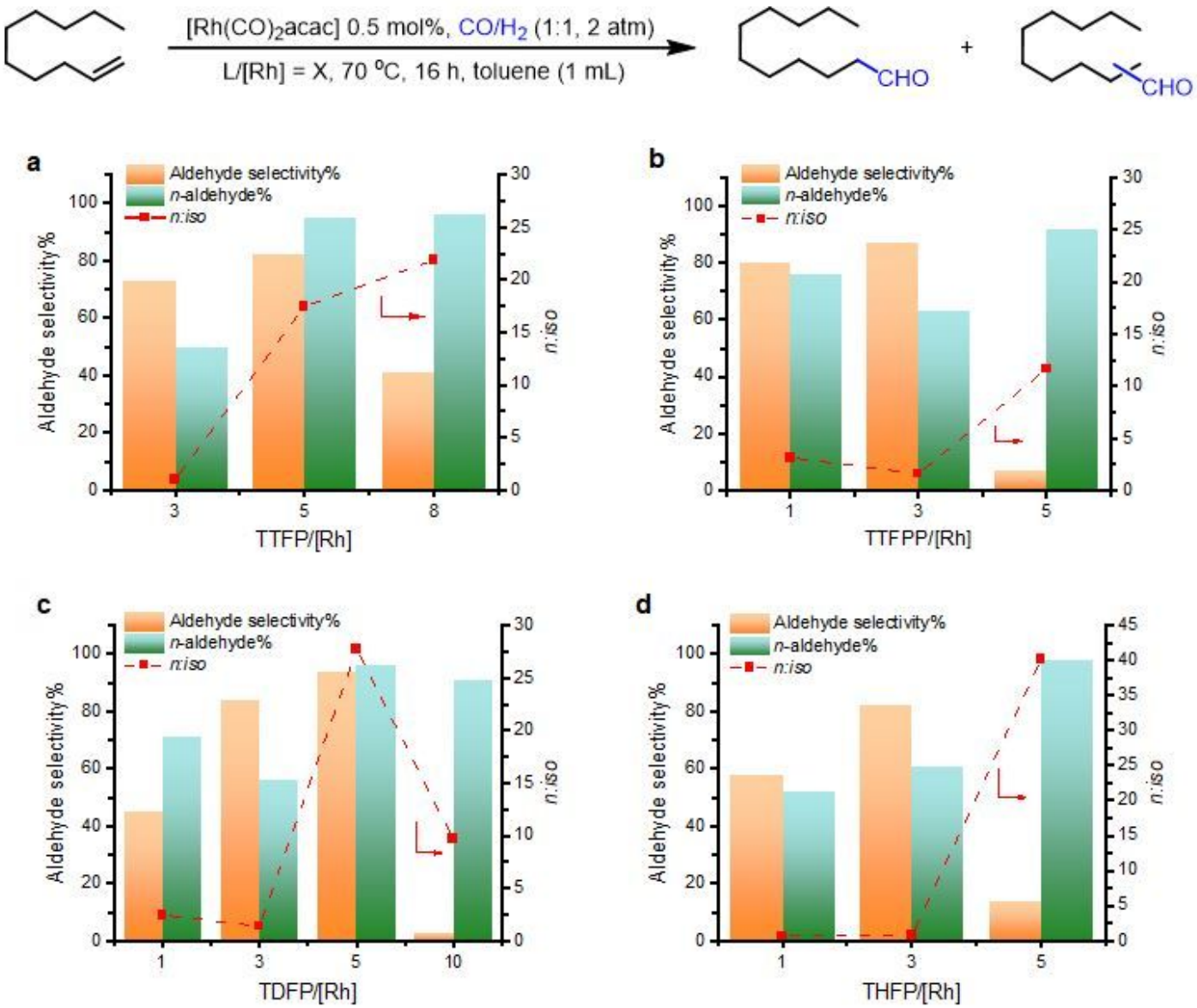

Figure 2

Optimizing the reaction conditions for the hydroformylation of 1-decene using various fluorine-containing monodentate phosphite ligands.

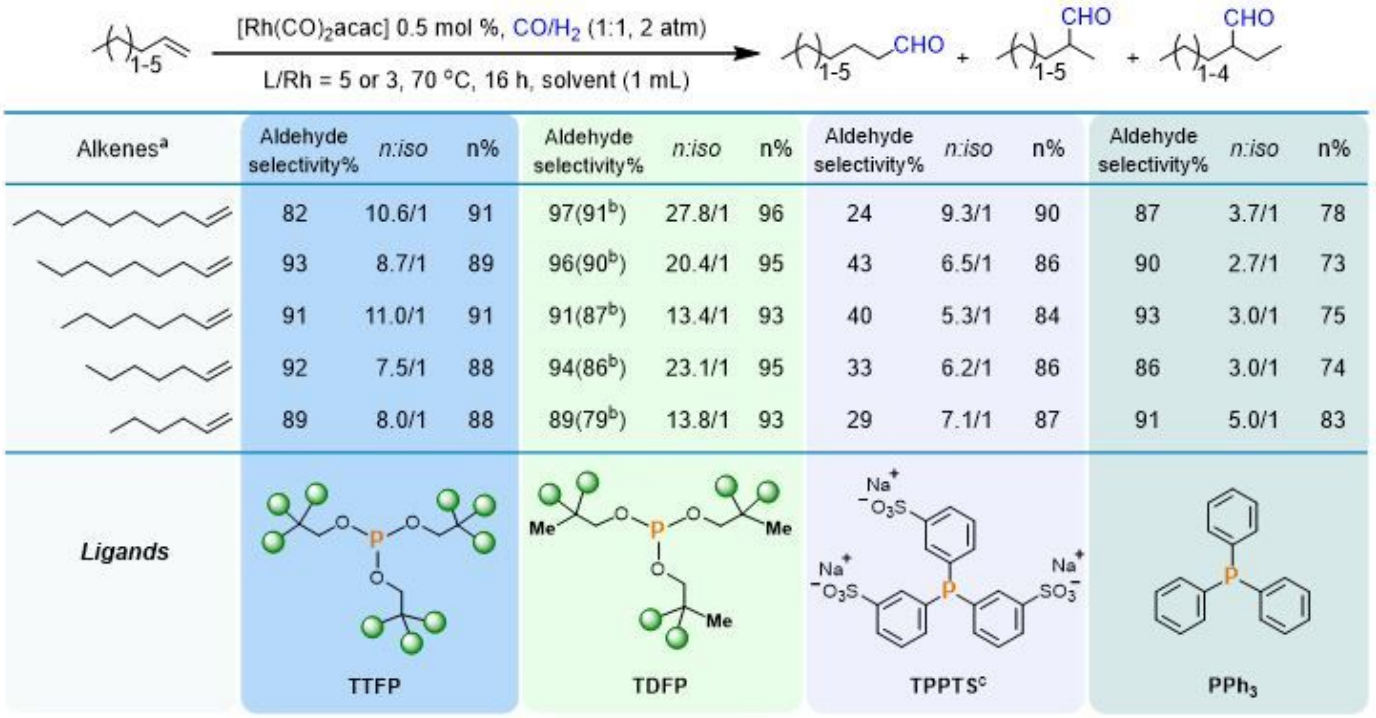

Figure 3

Regioselective hydroformylation of terminal olefins with fluorinated phosphites, PPh3 and the water-soluble TPPTS.

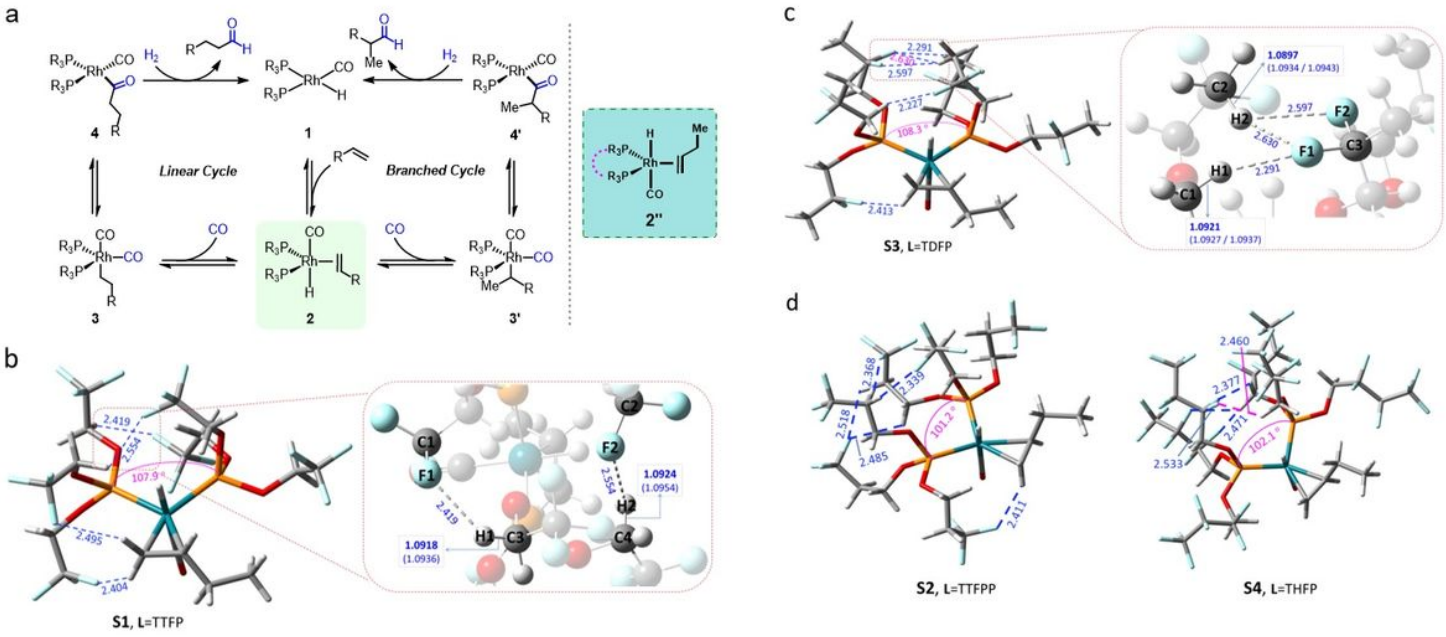

Figure 4

DFT-optimized structures for the 1-butene-coordinated intermediate 2". a, Wilkinson's catalytic cycle for the [Rh(L)2(CO)H]-catalyzed hydroformylation. b, DFT-optimized structure of the complex with TTFP. c,

DFT-optimized structure of the complex with TDFP. d, DFT-optimized structures of the complexes with TTFPP and THFP. Angles are given in degrees and bond distances in Å.

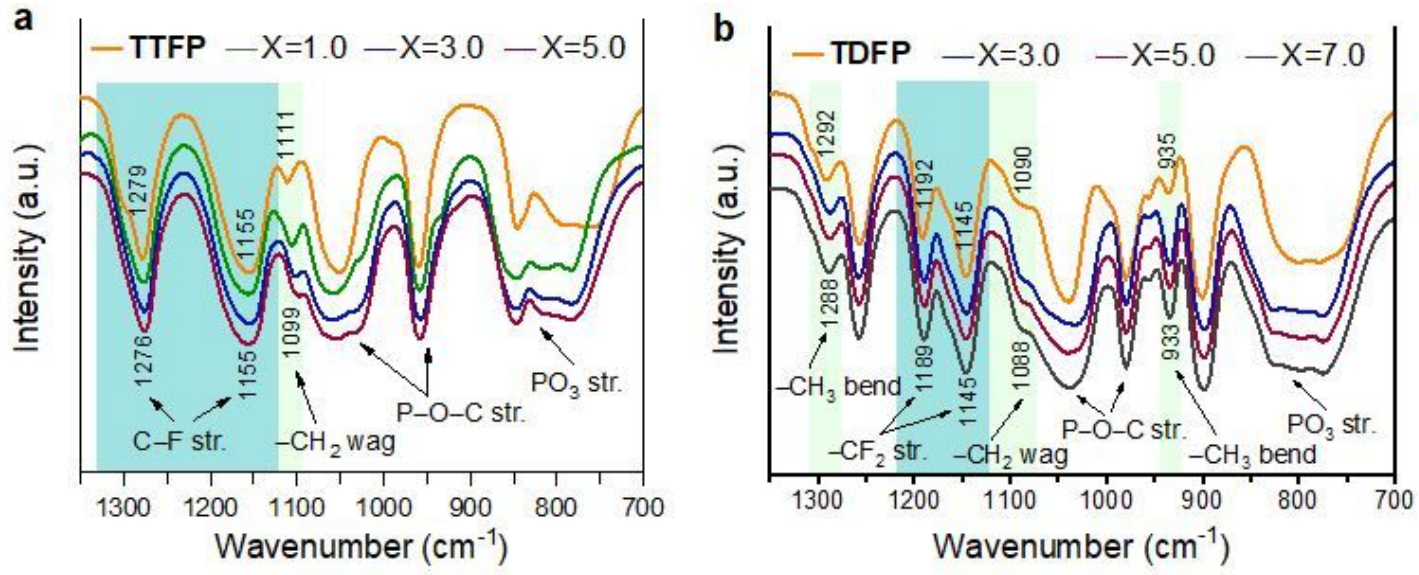

Figure 5

FTIR spectra of A) TTFP/[Rh] and B) TDFP/[Rh], where [Rh] is Rh(acac)(CO)2 and X is the ligand/[Rh] ratio.